Constraints Imposed by the Wilshire Methodology on Creep Rupture Data and Procedures for Testing the Validity of such Constraints: Illustration using 1Cr-1Mo-0.25V Steel

MARK EVANS

College of Engineering, Swansea University, Singleton Park, Swansea, SA2 8PP, UK.

Tel: +44(0)1792 295748; Fax: +44(0)1792 295676; Email: m.evans@swansea.ac.uk

ABSTRACT

A new parametric approach, termed the Wilshire equations, offer the realistic potential of being able to accurately life materials operating at in service conditions from accelerated test results lasting no more than 5,000h. These Wilshire equations contain discontinuities that have in the literature been interpreted either in terms of changing deformation mechanisms or changes in where deformation occurs within a material (i.e. within boundaries or crystals). This paper demonstrates that the rather restrictive nature of these discontinuities within the Wilshire equations can lead to problems in identifying an appropriate model for long term life prediction. An alternative framework is developed that removes these restrictions but still maintains the fundamental nature and characteristics of the Wilshire methodology. Further, when this alternative structure is applied to 1Cr-1Mo-0.25V steel, it produces more accurate and realistic looking long term predictions of the time to failure.

Keywords:

Creep, rupture time, Wilshire methodology, prediction

I. INTRODUCTION

In general, when selecting alloy steels for large-scale components used in power and petrochemical plants, decisions are based on the 'allowable creep strengths', normally calculated from the tensile stresses causing failure in 100,000h at the relevant service temperatures [1]. However, creep life measurements for structural steels show considerable batch to batch variability so, in Europe, tests up to 30,000 h have often been completed for five melts of each steel grade [2]. The development of a parametric approach, termed the Wilshire equations [3,4], offers the realistic potential of being able to accurately life materials operating at in service conditions from accelerated test results lasting no more than 5,000h. A plethora of recent publications have applied these equations to a range of different materials [5,6,7,8] and have provided evidence to suggest that data extrapolation from accelerated tests using these Wilshire equations is a realistic and attractive alternative to expensive long term testing. This opportunity is particularly exciting when considering the development of new materials for high temperature applications. Indeed a reduction in the development cycle for new steels was identified as the No.1 priority in the 2007 UK Strategic Research Agenda [9]).

The Wilshire equations [3,4] seem to avoid the unpredictable n value variations that are well known to exist when using the following power law expression for modelling creep properties as a function of stress and temperature

$$\dot{\varepsilon}_m = A^* (\sigma/\sigma_{TS})^n \exp(-Q^*_c/RT) \qquad [1]$$

where T is the absolute temperature, σ the stress, σ_{TS} the ultimate tensile strength, R the universal gas constant and Q^*_c the activation energy for self-diffusion. A^* and n are further parameters of the model. Q^*_c is normally estimated from the temperature dependency of $\dot{\varepsilon}_m$ at constant σ/σ_{TS}, whilst n is normally estimated from the normalised stress dependency of $\dot{\varepsilon}_m$ at constant T (often this power law model is expressed in a format that excludes the tensile strength).

In the Wilshire model, the unpredictable n variation is overcome by describing the stress and temperature dependencies of the minimum creep rate $\dot{\varepsilon}_m$ as

$$(\sigma/\sigma_{TS}) = \exp\left\{-k_2\left[\dot{\varepsilon}_m.\exp(Q^*_c/RT)\right]^v\right\} \qquad [2]$$

where k_2 and v are further model parameters. This equation provides a sigmoidal data presentation such that $\dot{\varepsilon}_m \to \infty$ as $(\sigma/\sigma_{TS}) \to 1$ (provided $v < 0$), whereas $\dot{\varepsilon}_m \to 0$ as $(\sigma/\sigma_{TS}) \to 0$. Wilshire and Battenbough [3] proposed a very similar expression to Eq. [2] for the stress and temperature dependencies of the time to failure, t_f

$$(\sigma/\sigma_{TS}) = \exp\left\{-k_1\left[t_f.\exp(-\rho Q^*_c/RT)\right]^u\right\} \qquad [3]$$

where ρ is often taken to be equal to unity and is the exponent in the Monkman – Grant relation [10]. To link this Wilshire expression to that for the minimum creep rate in Eq. [2], use must be

made of this Monkman and Grant relation which is an empirical relationship that exist between the time to failure and the minimum creep rate. This relationship is often expressed in the form

$$\dot{\varepsilon}_m^{\rho} t_f = M \qquad [4]$$

where M is a material specific constant. Essentially, the value for M measures what the strain at rupture would have been had the material deformed at the minimum creep rate over its whole life. Monkman and Grant believed M to be independent of the test conditions.

Rearranging Eq. [4] for $\dot{\varepsilon}_m$ and substituting the resulting expression into Eq. (2) gives

$$(\sigma/\sigma_{TS}) = \exp\left\{-k_2 M^{v/\rho}\left[t_f.\exp(-\rho Q_c^*/RT)\right]^{v/\rho}\right\} \qquad [5a]$$

In terms of the Wilshire expression in Eq. [2], it must follow that in Eq. [3] the value for k_1 and u should equal

$$u = -v/\rho \quad ; \quad k_1 = k_2 M^{v/\rho} \qquad [5b]$$

This paper aims to highlight a number of short comings associated with this Wilshire approach to estimating the life of materials operating at high temperatures. Some of these concerns are relatively minor in that they relate to estimation issues, but others are more serious in that they relate to restrictions the Wilshire equations impose on the deformation mechanism leading to creep failure and also to the unrealistic nature of the iso-thermal prediction lines produced by these equations. Specifically, the Wilshire equation allows for dramatic changes in the parameters of the model, including the activation energy, at specific values for the normalised stress. It does not allow such discontinuities with respect to temperature. To the extent to which such discontinuities reflect changing deformation mechanisms or changes in where deformation occurs within a material (within boundaries or crystals), the Wilshire equations do not therefore allow for mechanisms to change with respect to temperature – despite such changes being well recognised. The abruptness of these discontinuities in the Wilshire model also results in kink-like iso-thermal predictions where ideally, these iso-thermal projections should be smooth in appearance. The paper then suggest how these limitations can be overcome by providing a new framework for modelling and estimation whilst remaining within the formulisation of the Wilshire approach. These limitations and modification will be illustrated using 1Cr1Mo0.25V – the data set on which is described in the next section.

II. THE DATA

To illustrate the points discussed above, the present study features forged 1Cr-1Mo-0.25V steel for turbine rotors and shafts. For multiple batches of this bainitic product, both the creep and creep fracture properties have been documented comprehensively by the National Institute for Materials Science (NIMS), Japan [11]. NIMS creep data sheet No. 9B includes information on nine batches of as tempered 1Cr-1Mo-0.25V steel. Table I gives the chemical composition of each of these batches. Specimens for the tensile and creep rupture tests were taken radially from the ring shaped samples which were removed from the turbine rotors. Each test specimen had a diameter of 10mm with a gauge length of 50mm.

Table I. Composition and Heat Treatment of 1Cr-1Mo -0.25V Steel

These specimens were tested at constant load over a wide range of conditions: 333 MPa - 47MPa and 723K (450ºC) – 923K (650 ºC). In addition to minimum creep rate ($\dot{\varepsilon}_m$) and time to failure (t_F) measurements, values were also given of the times to attain various strains (t_e) - 0.005, 0.01, .02 and 0.05 over this range of test conditions. Also reported were the values of the 0.2% proof stress (σ_Y) and the ultimate tensile strength (σ_{TS}) determined from high strain ($\sim 10^{-3}$ s^{-1}) tensile tests carried out at the creep temperatures for each batch of steel investigated.

III. TRADITIONAL APPROACH TO ESTIMATING k_1, u AND Q^*_c

Eq. [3] can be linearized through the use of a double logarithmic transformation of the normalised stress as follows

$$\ln[t_f.\exp(-\rho Q_c^*/RT)] = -\frac{\ln(k_1)}{u} + \frac{1}{u}\sigma^* \quad \text{with} \quad \sigma^* = \ln[-\ln(\sigma/\sigma_{TS})] \qquad [6]$$

Over the last six years, this Wilshire equation has been applied to many power generating and aerospace materials [4-8]. However, in all these studies it has been found that when $\ln[t_f.\exp(-\rho Q_c^*/RT)]$ is plotted against $\ln[-\ln(\sigma/\sigma_{TS})]$ two or more distinct straight line segments are present. That is, there appear to be distinct regions for the normalised stress, typically referred to as regions of "high" and "low "stress (or low, medium and high stress when three regions are present). This complicates the procedure for finding values for the unknown parameters k_1, u and Q^*_c. However, it is important to realise that such discontinuities do not invalidate the extrapolation from short term data using Eq. [6] because these regions are the same in short and long term data sets on a given material (unlike the n value in Eq. [1]). For example, the reader is referred to Wilshire and Whittaker [5] for an application to 2.25Cr-1Mo steels where three distinct regions were identified by these authors and Wilshire and Scharning [4] for an application to 1Cr-1Mo-0.25V steel where only two distinct regions were identified.

Whittaker and Wilshire [5] proposed the following procedure for estimating the unknown parameters in Eq. [6]. First, the presence of distinct regions is deliberately ignored. ρQ^*_c is then determined as the value that minimises the least-squares fitting error that superimposes the individual data points on a plot of $\ln[t_f\exp(-\rho Q_c^*/RT)]$ against $\ln[-\ln(\sigma/\sigma_{TS})]$ onto the best straight line given by Eq. [6]. The authors describe this as an iterative procedure whereby a value for ρQ^*_c is guessed at (based on past activation energy studies presumably) which then enables the variable on the left hand side of Eq. [6] to be quantified. This constructed variable is then regressed on σ^* to determine a value for k_1 and u (using least squares principles). This process is repeated using a range of values for ρQ^*_c around the initially guessed value and the correct value for ρQ^*_c is taken to be that which results in the smallest least squares fitting error. Using this value for ρQ^*_c, a plot of $\ln[t_f.\exp(-\rho Q_c^*/RT)]$ against $\ln[-\ln(\sigma/\sigma_{TS})]$ will reveal visually where the break(s) in the straight line relationship between these two variables exists. Having identified all the straight line regions or breaks, the above approach is repeated on each region of data separately to determine the values for k_1, u and ρQ^*_c that are most appropriate for each region.

IV. AVOIDING SUBJECTIVITY

The first issue with this estimation procedure is that the authors don't explicitly state the method used for minimising the least squares fitting error. Presumably, having split the data into different stress regions, the standard least squares formulas are used to select values for k_1, u and ρQ^*_c so as to minimise the sums of the squares of the fitting error, or Σe^2

$$\ln[t_f] - \rho Q^*_c \frac{1}{RT} = -\frac{\ln(k_1)}{u} + \frac{1}{u}\sigma^* + e \qquad [7]$$

in each sub set of data (where the summation is over all the data points within the subset of data). However, this is a little too subjective as the precise point where the breaks occur should be part of the estimation procedure itself, i.e. the break points should not be guessed at from a visual inspection of a plot of $\ln[t_f \exp(-\rho Q^*_c/RT)]$ against $\ln[-\ln(\sigma/\sigma_{TS})]$. Evans [12] put forward a formal procedure for doing exactly this through the use of binary variables. So when one break is present, Eq. [7] can be written as

$$\ln(t_f) = -\frac{\ln(k_1)}{u} + \frac{1}{u}\sigma^* + \rho Q^*_c(1/RT) + \Delta_1[\sigma^* - \sigma^*_{kink}]D_1 + \Delta_2(D_2/RT) + e \qquad [8]$$

where $\sigma^*_{(kink)}$ is the value for σ^* at which the above described discontinuity occurs, i.e. at which the values for u and k_1 change. D_1 and D_2 are binary variables such that $D_1 = D_2 = 0$ when $\sigma^* \geq \sigma^*_{(kink)}$ and unity otherwise. Δ are further parameters to be estimated. Thus a simple grid search is conducted whereby the parameters in Eq. [8] are estimated for all values of $\sigma^*_{(kink)}$ in the range defined by the maximum and minimum values for σ^*. For each value of $\sigma^*_{(kink)}$, Eq. [8] will have a different error sum of squares associated with it, i.e. Σe^2 varies with $\sigma^*_{(kink)}$. The estimated values for u, ρQ^*_c, k_1, Δ_1, Δ_2 and $\sigma^*_{(kink)}$ are then those that produce the smallest error sum of squares. Eq. [8] implies that below $\sigma^*_{(kink)}$, 1/u changes to $1/u + \Delta_1$ and $-\ln(k_1)/u$ will change to $-\ln(k_1)/u - \Delta_1\sigma^*_{(kink)}$. This allows k_1 and u to change at some specific value for the normalised stress. Additionally, below $\sigma^*_{(kink)}$, ρQ^*_c changes to $\rho Q^*_c + \Delta_2$. This technique is easily generalised when two or more break points exist.

As an illustration, Eq. [8] was applied to the 1Cr-1Mo-0.25V data set described above. The least squares estimates for the unknown parameters in this equation were

$$\ln(t_f) = \underset{[-44.2]}{-22.8681} + \underset{[45.8]}{8.4509}\sigma^* + \underset{[79.8]}{283{,}670}(1/RT) - \underset{[-20.7]}{4.2275}(\sigma^* + 0.1907)D_1 + \underset{[3.2]}{1819.57}(D_2/RT)$$

$$R^2 = 97.49\% \qquad [9a]$$

where student t values, that test the null hypothesis that the true value for the unknown parameters are zero, are given in parenthesis, and R^2 is the coefficient of determination. These estimates imply that the break occurs at $\sigma^* = -0.1907$ or at a normalised stress of $\sigma/\sigma_{TS} = 0.44$. The student t values suggest that all the parameters are significantly different from zero at the 5% significance level so that the k_1, u and Q^*_c all appear to change above and below this break

point stress. For this 1Cr-1Mo-0.25V data set, the values for M and ρ in the Monkman - Grant relation were estimated at

$$\dot{\varepsilon}_{m}^{0.9687} t_f = 0.052 \qquad [9b]$$

using ordinary least squares. So with ρ estimated as 0.9687, the activation energy is approximately 283,670/0.9687 ≈ 293 kJmol^{-1} when $\sigma^* \geq \sigma^*_{(kink)}$. When σ^* then drops below the critical normalised stress this activation energy changes by approximately 2 kJmol^{-1}, which whilst statistically significant, is a small change. Again, at this break point stress, the reciprocal of u changes by -4.2278 from 8.4509 – which in comparison to the activation energy change is a relatively big change. These estimates are in very good agreement with the values quoted in Wilshire and Scharning [4]. The R^2 value shows that just over 97% of the variation in the log of the time to failure can be explained by the variables on the right hand side of Eq. [8].

This is all visualised in Figure 1. In Figure 1 the break at a normalised stress of 0.44 is visually apparent and the predictions given by Eq. [9a] are shown by the segmented line. The figure reveals that there is a tendency for this model to underestimate the failure times recorded at the lower stress levels at 823K (550°C) . It can be seen from Figure 1 that the filled triangles at normalised stresses below 0.4 are consistently below the solid line corresponding to the models predictions – implying, given the nature of the constructed variable on the horizontal axis, an underestimate of t_f. This is perhaps more clearly seen in Figure 4, where failure time itself is shown on the horizontal axis. The models predictions given by the solid line at 823K (550°C) drifts further towards the lower end of the experimental failure times as stress diminishes.

Fig. 1 - Dependence of $\ln[t_f \exp(-\rho Q_c^*/RT)]$ on $\ln[-\ln(\sigma/\sigma_{TS})]$ for 1Cr-1Mo-0.25V steel at 723K (450°C) to 948K (675°C). (Failure time t_f is in seconds, stress σ is in MPa, and Temperature T is the absolute temperature).

V. ALLOWING FOR STRESS AND TEMPERATURE DEPENDENT BREAKS

The second and more serious issue is that the estimation procedure used by Whittaker and Wilshire [5], allows changes in the value for k_1, u and the activation energy to be exclusively stress dependent. At first sight this does not appear to be a problem, as for example, Wilshire and Whittaker [5] attribute this in their 2.25Cr-1Mo study to changing regions where deformation occurs within the material. For this material, these authors suggests that no transition takes place from dislocation to diffusional creep mechanisms with decreasing applied stress. Instead, dislocation creep processes are rate controlling at all stress levels, even though the detailed dislocation processes vary in different stress regimes. Thus, with 2.25Cr-1Mo steels, the creep and creep fracture properties differ above and below $\sigma \approx \sigma_Y$ (where σ_Y is the yield stress). According to Wilshire and Whittaker [5], when $\sigma > \sigma_Y$, so that the initial strain on loading has both elastic and plastic components, creep is controlled by the generation and movement of dislocations within the grains. In contrast, when $\sigma < \sigma_Y$, so that the strain on loading has essentially only an elastic component, new dislocations are not generated within the grains, so creep occurs within the grain boundary zones, i.e. by grain boundary sliding and

associated deformation in the grain regions adjacent to the boundaries. Hence, the creep rates when $\sigma < \sigma_Y$ are slower and the creep lives are longer than expected by direct extrapolation of $\dot{\varepsilon}_m$ data obtained when $\sigma < \sigma_Y$.

Another change in creep and creep rupture behaviour occurs when σ approximately equals $0.2\sigma_{TS}$. With this material, a transformation from bainite to ferrite and coarse carbide particles takes place in long-term tests at the highest creep temperatures. In these cases, because of the loss of creep resistance caused by this transformation, the $\dot{\varepsilon}_m$ values are faster when $\sigma < 0.2\sigma_{TS}$ than would be predicted by extrapolation of data collected at intermediate σ levels. These authors have provided similar explanation for the observed breaks in other power generating materials as well.

However, the conventional approach to describing creep is in terms of deformation mechanism diagrams that typical show how deformation mechanisms depend not just on stress but also on temperature. A classic presentation of a deformation mechanism diagram, taken from Ashby and Jones [13], is shown in Figure 2. Creep strain can be caused by different mechanisms that take place in different regions of the material depending on both stress and temperature. Yet, the estimation procedure describe by Whittaker and Wilshire [5] only allows for a change in mechanism with respect to stress and so may not identify the correct form of Eq. [7]. A more general estimation technique that allows for the possibility of breaks at differing stresses and temperatures is required.

Fig. 2 - Deformation mechanisms at different stresses and temperatures. Ashby and Jones [13].

Again working with the 1Cr-1Mo-0.25V data described above, this potential for model mis-specification can be easily illustrated. Instead of looking for breaks with respect to stress, it is arguably just as valid to look for breaks with respect to temperature. Deformation mechanism diagrams for example, typically suggest a transition from dislocation creep that is predominant in the bulk crystals to it being predominant along grain boundaries as the temperature is lowered as well as when stress is lowered. To search for a break as a function of temperature, the failure time is compensated by the normalised stress rather than the temperature. Placing all terms not containing temperature on the right hand side of Equation [7] and all other terms on the left hand side, leaves a plot of $\ln[t_f \exp(-\sigma^*/u)$ against 1/RT. In the space defined by such a plot, a search can be carried out to find the critical temperature at which the activation energy and the parameters k_1 and u change. So when one break is present in such a plot, the regression equation has the form

$$\ln(t_f) = -\frac{\ln(k_1)}{u} + \frac{1}{u}\sigma^* + \rho Q_c^*(1/RT) + \Delta_1\left[\frac{1}{RT} - \left(\frac{1}{RT}\right)_{kink}\right]D_1 + \Delta_2(D_2\sigma^*) + e \quad [10]$$

where $(1/RT)_{kink}$ is the value for 1/RT at which the above described discontinuity occurs, i.e. at which the value for Q^*_c changes. D_1 and D_2 are binary variables such that $D_1 = D_2 = 0$ when $1/RT \leq 1/RT_{kink}$ and unity otherwise. Δ are further parameter to be estimated. Thus a simple grid search is conducted where by the parameters in Eq. [10] are estimated for all values of

$(1/RT)_{kink}$ in the range defined by the maximum and minimum values for 1/RT in the experimental data set. For each value of $(1/RT)_{kink}$, Eq. [10] will have a different error sum of squares associated with it. The estimated values for u, ρQ^*_C, k_1, Δ_1, Δ_2 and $(1/RT)_{kink}$ are then those that produce the smallest error sum of squares. Eq. [10] implies that above $(1/RT)_{kink}$, 1/u changes to $1/u + \Delta_2$ and $-\ln(k_1)/u$ will change to $-\ln(k_1)/u - \Delta_1(1/RT)_{kink}$ - hence allowing k_1 and u to change at some specific value for the absolute temperature. Additionally, above $(1/RT)_{kink}$, ρQ^*_c changes to $\rho Q^*_c + \Delta_1$. This technique is easily generalised when two or more break points exist.

The least squares estimates for the unknown parameters in Eq. [10] are

$$\ln(t_f) = -27.2525 + 4.7513\sigma^* + 309{,}679(1/RT) - 48{,}445\left[\frac{1}{RT} - 0.000146\right]D_1 + 2.4652(D_2\sigma^*)$$

[-39.6] [52.6] [63.5] [-5.0] [17.3]

$R^2 = 97.30\%$

[11]

so that the R^2 value is maximised when $(1/RT)_{kink} = 0.000146$ which corresponds to an absolute temperature of 823K (550°C). Whilst this break point in not so visually apparent in Figure 3 as is the break in Figure 1, (due to the additional scatter present in the data shown in Figure 3), it is non the less real or statistically significant as revealed by the student t values shown in parenthesis in Eq. [11]. For example, the student t value for Δ_1 (of -5) exceeds its critical value at the 5% significance level, revealing that at $(1/RT)_{kink}$ = 0.000146 the activation energy undergoes a statistically significant change. A statistically significant change in the parameter u is also present at this break point.

At the critical temperature of 823K (550°C) the reciprocal of u changes by 2.4652 from 4.7513. At the critical temperature of 823K (550°C) the activation energy changes by -48,445 $Jmol^{-1}$ from 309.679 / 0.9687 ≈ 320 $kJmol^{-1}$. The R^2 value shows that just over 97% of the variation in the log of the failure time can be explained by the variables on the right hand side of Eq. [10]. This is all visualised in Figure 3, where the break at a 1/RT = 0.000146 is visually apparent and a noticeable change in both the activation energy and the values for k_1 and u occurs.

Fig. 3 - Dependence of $\ln[t_f.\exp(-\sigma^*/u)]$ on $1/RT$ for 1Cr-1Mo-0.25V steel at 723K (450°C) to 948K (675°C). (Failure time t_f is in seconds, stress σ is in MPa, and Temperature T is the absolute temperature).

Depending on whether a break is searched for with respect to stress or temperature two very different models emerge, both of which have similar fits to the data – just over 97% for the R^2 value:

$$(\sigma/\sigma_{TS}) = \exp\left\{14.969\left[t_f.\exp(-\rho 292{,}836/RT)\right]^{0.118}\right\} \quad \text{when} \quad \sigma/\sigma_{TS} \le 0.44$$

$$(\sigma/\sigma_{TS}) = \exp\left\{271.883\left[t_f.\exp(-\rho 294{,}714/RT)\right]^{0.237}\right\} \quad \text{when} \quad \sigma/\sigma_{TS} > 0.44$$

or

$$(\sigma/\sigma_{TS}) = \exp\left\{16.368\left[t_f.\exp(-\rho 269{,}657/RT)\right]^{0.139}\right\} \quad \text{when} \quad T \le 823K$$

$$(\sigma/\sigma_{TS}) = \exp\left\{309757\left[t_f.\exp(-\rho 319{,}686/RT)\right]^{0.210}\right\} \quad \text{when} \quad T > 823K$$

But the physical interpretation that could be given to each has to be very different for these equations to make sense. In the second model, the rise in Q^*_c towards 320 kJmol^{-1} could reflect the fact that creep is controlled more by lattice self-diffusion than grain boundary diffusion above 823K (550°C) – as the activation energy is higher for the bulk of the material. However, the first model suggests a very different set of phenomenon. The value for the activation energy and the relatively small change in this activation energy with respect to stress is consistent with creep being controlled by lattice self-diffusion. However, below the critical stress, the longer duration of the tests in this regime leads to an evolution of the as received bainitic microstructure that progressively reduces creep resistance. This evolution then explains the observed change in the value for k_1 and u. Clearly these two models are incompatible with each other in that only one of the explanations can be correct (and also the implied activation energy for lattice diffusions is different in each approach). This problem stems from searching for breaks with respect to only one of the test variables.

VI. DISCONTINUITIES

Finally, and related to this last point, is the fact that in reality changes in mechanism are not as abrupt as that implied by the Wilshire equations. The boundaries on deformation mechanism diagrams represent the conditions under which two or more creep processes contribute equally towards creep strain. It should therefore be expected that the parameters in the Wilshire equation should change gradually as movement from a low to a high stress regime takes place – and not abruptly at a break point as is usually visualised on Wilshire type plots of $\ln[t_f.\exp(-\rho Q^*_c/RT)]$ against $\ln[-\ln(\sigma/\sigma_{TS})]$. Another way of saying this is that on the iso-thermal prediction curves produced using the Wilshire equations, an abrupt change occurs at a specific stress for a given temperature. This is completely artificial as what should actually happen is a smooth and gradual change in the slope of the predicted iso-thermal curve as this stress point is approached and passed. This is visualised in Figure 4 where the solid curves are the creep lives predicted by Eq. [9a] at two selected temperatures – 823K (550°C) and 873K (600°C). These predictions were obtained using the average (over all batches) tensile strength at these two temperatures. The observed discontinuity occurring at a normalised stress of 0.44 reflects both the change in k_1 and u and the smaller change in the activation energy. This discontinuity occurs at slightly different stresses at each temperature because the tensile strength is temperature dependent. The dashed curves are the creep lifes predicted by Eq. [11] at these selected temperatures. Because a discontinuity occurs at a specific temperature, these iso-thermal predictions have no kink. But the resulting predictions at lower stresses are very different, especially at 823K (550°C) where one model appears to be underestimating the time to failure at the lowest stresses and the other is over-estimating at these stresses. Yet overall, the two models produce similar fits over the whole stress range and which to select is not obvious.

Fig. 4 - Predicted times to failure obtained using Eq. [9a] and Eq. [11] for specimens tested at 823K (550°C)and 873K (600°C).

VII. MODIFIED MODEL

A. The Model

The discontinuity problem illustrated above can be overcome by allowing for a gradual change. The best way to explain this is to look at the simplest possibility first, namely where a change occurs with respect to the normalised stress only, so that

$$\ln[t_f] = w_1\left[a_1 + b_1\sigma^* + d_1\frac{1}{RT}\right] + [1 - w_1]\left[a_2 + b_2\sigma^* + d_2\frac{1}{RT}\right] + e \qquad [12a]$$

where

$$w_1 = \frac{1}{1 + \exp[-\beta_1(\sigma^* - \sigma^*_{kink})]} \qquad [12b]$$

The interpretation of this model is as follows. When $\sigma^* = \sigma^*_{(kink)}$, w_1 will equal 0.5. Then, two different creep processes (or groups of processes) contribute equally towards the overall minimum creep rate and rupture time. Then as σ^* continues to fall below $\sigma^*_{(kink)}$, w_1 tends to unity and $1\text{-}w_1$ tends to zero so that the creep rate is increasingly determined by one of these creep mechanisms. When $w_1 = 1$, the creep rate is determined only by a single deformation mechanism. In effect w_1 measures the dominance of a particular deformation mechanism. Then d_1 can be interpreted as the activation energy associated with one mechanism, whilst d_2 is the activation energy associated with the other mechanism.

Similarly, b_1 can be interpreted as the value for 1/u associated with this mechanism, whilst b_2 is the value for 1/u associated with the other mechanism. a_1 is thus related to the value for k_1 in the first mechanism and so on. For example, as σ^* continues to rise above $\sigma^*_{(kink)}$ dislocation movements may become increasingly confined to the grain boundaries where the activation energy given by d_2 applies. Then as σ^* falls below $\sigma^*_{(kink)}$ the higher stresses may allow dislocation movements to occur within the crystal structure itself, where the activation energy will be at a higher value given by d_1 – and this will dominate creep as σ^* becomes very small.

This model allows for a gradual evolution in the deformation mechanisms determining creep as stress changes and so avoids the abrupt discontinuities of the original Wilshire model. To account for changing mechanisms with respect to temperature, this model can be appropriately generalised as follows

$$\begin{aligned}\ln[t_f] = {} & w_1\left[a_1 + b_1\sigma^* + d_1\frac{1}{RT}\right] + w_2\left[a_2 + b_2\sigma^* + d_2\frac{1}{RT}\right] \\ & w_3\left[a_3 + b_3\sigma^* + d_3\frac{1}{RT}\right] + w_4\left[a_4 + b_4\sigma^* + d_4\frac{1}{RT}\right] + e\end{aligned} \qquad [13a]$$

where

$$w_1 = z_1 z_2 \; ; \; w_2 = z_1(1-z_2) \; ; \; w_3 = (1-z_1)z_2 \; ; \; w_4 = (1-z_1)(1-z_2) \qquad [13b]$$

and

$$z_1 = \frac{1}{1+\exp[-\beta_1(\sigma^* - \sigma^*_{kink})]} \quad ; \quad z_2 = \frac{1}{1+\exp\left[-\beta_2\left\{\frac{1}{RT} - \left(\frac{1}{RT}\right)_{kink}\right\}\right]} \qquad [13c]$$

The idea behind Eq. [13b,c] is that z_1 and z_2 again measure the dominance of creep mechanisms that are stress and temperature dependent, respectively. In this model there are now four distinct regions. One region is where the transformed stress is below $\sigma^*_{(kink)}$ and the reciprocal of the absolute temperature is below $(1/RT)_{kink}$. In this region a creep mechanism (or group of mechanisms) will dominate and the degree of dominance is determined by the product of z_1 and z_2, i.e. by w_1. Essentially, z_1 is measuring the extent to which σ^* is below $\sigma^*_{(kink)}$ and z_2 is measuring the extent to which 1/RT is below $(1/RT)_{kink}$. The extent to which both σ^* is below $\sigma^*_{(kink)}$ and 1/RT is below $(1/RT)_{kink}$ is the product of z_1 and z_2 (in much the same way as the probability of event A and event B occurring is the product of their individual probabilities for independent events). Thus as σ^* drops further below $\sigma^*_{(kink)}$ and as 1/RT drops further below$(1/RT)_{kink}$, z_1 and z_2 get closer to unity and so too does w_1 and creep is then dominated by the mechanism(s) associated with high stresses and high temperatures. The activation energy associated with this mechanism is then given by d_1 and b_1 gives the value for 1/u associated with this mechanism.

Eq. [13b,c] are such that all the w values sum to unity. In this model there are also creep strains determined by a mechanism (or mechanisms) associated with low stresses and temperatures, a low stress but a high temperature and a high stress but a low temperature. Further, given the S shaped nature of Eq. [13c] the degree to which these mechanisms dominate evolves slowly with changing stresses and temperatures with all mechanisms contributing equally at $\sigma^*_{(kink)}$ and $(1/RT)_{kink}$. What is useful about this model is that if the estimated value for β_1 and β_2 are very large in absolute terms, the S shaped curves become very steep around points $\sigma^*_{(kink)}$ and $(1/RT)_{kink}$. Then this model takes on the sharp discontinuity properties associated with the original Wilshire model. This framework therefore offers a means of testing the validity of this Wilshire property by looking at the magnitude of β_1 and β_2.

B. Estimation

It should be apparent from this modification that the parameters requiring estimation are a_i, b_i, d_i for i = 1 to 4, $\sigma^*_{(kink)}$, $(1/RT)_{kink}$, β_1 and β_2. Estimation is actually relatively straight forward, but iterative. On the first iteration values for $\sigma^*_{(kink)}$, $(1/RT)_{kink}$, β_1 and β_2 are guessed at. This allows values for w_i to be calculated which in turn allows the following new variables to be calculated: w_i, $w_i\sigma^*$ and w_i/RT for i = 1 to 4. The following least squares regression can then be carried out

$$\ln[t_f] = a_i \sum_{i=1}^{4} w_i + b_i \sum_{i=1}^{4} w_i \sigma^* + d_i \sum_{i=1}^{4} \frac{w_i}{RT} + e \qquad i = 1,\ldots,4 \qquad [14]$$

where the parameters a_i, b_i and d_i are chosen so as to minimise Σe^2. Notice this is a standard multiple regression problem with no constant term included in the regression equation. Then a standard Gauss – Newton non-linear optimisation algorithm can be used to search for other values of $\sigma^*_{(kink)}$, $(1/RT)_{kink}$, β_1 and β_2 that further reduce the value for Σe^2 in Eq. [14]. In this way the optimal values for all parameters can be found. Or, alternatively, a grid search over all values for $\sigma^*_{(kink)}$ and $(1/RT)_{kink}$ could be carried out to find the combination that minimises Σe^2 in Eq. [14]. These approaches are easily implemented using the Solver option in Microsoft Excel – 2013- for example.

C. Illustration

As an illustration, Eqs. [13] were applied to the 1Cr-1Mo-0.25V data set described above. The estimates for $\sigma^*_{(kink)}$ and $(1/RT)_{kink}$ were -0.190 and 0.00014617 respectively. Likewise, the estimates for β_1 and β_2 are respectively -25.01 and -481.13. These estimates for the break points closely coincide with those estimated in Eqs. [9a,11], whilst the values for β_1 and β_2 suggest a gradual transition with respect to stress, but a rather abrupt transitions with respect to temperature. The complete estimated model is then given by

$$\begin{aligned}\ln[t_f] = {} & w_1\left[-20.55 + 6.22\sigma^* + 265{,}642\,\frac{1}{RT}\right] + w_2\left[-25.73 + 4.45\sigma^* + 299{,}252\,\frac{1}{RT}\right] \\ & \quad [-4.8]\quad [8.9]\qquad [9.3] \qquad\qquad\qquad [-25.5]\ [45.2]\qquad [39.9] \\ & w_3\left[-11.14 + 8.13\sigma^* + 206{,}486\,\frac{1}{RT}\right] + w_4\left[-7.19 + 7.66\sigma^* + 170{,}711\,\frac{1}{RT}\right] + e \\ & \quad [-4.2]\quad [39.4]\qquad [12.0] \qquad\qquad\qquad [-1.9]\ [11.7]\qquad [6.3] \\ R^2 = {} & 99.98\%\end{aligned} \tag{15}$$

where

$w_1 = z_1 z_2$; $w_2 = z_1(1-z_2)$; $w_3 = (1-z_1)z_2$; $w_2 = (1-z_1)(1-z_2)$

and

$$z_1 = \frac{1}{1+\exp[-25.011(\sigma^* + 0.1900)]} \quad ; \quad z_2 = \frac{1}{1+\exp\left[-481.126\left\{\frac{1}{RT} - 0.00014617\right\}\right]}$$

This model is capable of explaining over 99.9% of the variation in the log times to failure, where w_1 measures the extent to which deformation is dictated by the failure mechanism(s) associated with the lowest stresses and temperatures in the data set, through to w_4 which measures the extent to which deformation is dictated by the failure mechanism(s) associated with the highest stresses and temperatures in the data set. The student t values are

shown in parenthesis in Eq. [15] and imply that all the estimated parameters are statistically different from zero at the 5% significance level. These t values can be used to construct % confidence intervals for the estimated parameters assuming that these estimates follow a normal distribution. For example, 99% confidence intervals are given by

$a_1 \in (-31.7 \text{ to } -9.4)$; $a_2 \in (-28.3 \text{ to } -23.10)$

$a_3 \in (-18.1 \text{ to } -4.2)$; $a_4 \in (-16.9 \text{ to } 2.5)$

$b_1 \in (4.4 \text{ to } 8.0)$; $b_2 \in (4.2 \text{ to } 4.7)$

$b_3 \in (7.6 \text{ to } 8.7)$; $b_4 \in (6.0 \text{ to } 9.4)$

$d_1 \in (191{,}747 \text{ to } 339{,}537)$; $d_2 \in (279{,}757 \text{ to } 318{,}747)$

$d_3 \in (161{,}638 \text{ to } 251{,}334)$; $d_4 \in (100{,}523 \text{ to } 240{,}899)$

Taking first the confidence intervals for b_i. The overlap of the intervals for b_1 and b_2 and the intervals b_3 and b_4 suggest that there is no significant change in the stress relationship above and below $(1/RT)_{kink} = 0.00014617$. On the other hand, the non overlap of the intervals for b_1 and b_3 and the intervals b_2 and b_4 suggest that there is a significant change in the stress relationship above and below $\sigma^*_{(kink)} = -0.190$. A similar conclusion holds for the activation energy as well. The overlap of the intervals for d_1 and d_2 and the intervals b_3 and b_4 suggest that there is no significant change in the activation energy above and below $(1/RT)_{kink} = 0.00014617$. On the other hand, the non overlap of the intervals for d_2 and d_4 and the intervals d_2 and d_3 suggest that there is a significant change in the activation energy above and below $\sigma^*_{(kink)} = -0.190$.

These results suggests that a suitable parsimonious model of the creep data is that of the simplified version given by Eq. [12]. Estimating this model resulted in the following equation

$$\ln[t_f] = w_1\left[\underset{[-13.1]}{-14.4662} + \underset{[15.7]}{5.5140}\,\sigma^* + \underset{[27.2]}{211{,}834}\,\frac{1}{RT}\right] + [1-w_1]\left[\underset{[-46.1]}{-28.2100} + \underset{[34.3]}{4.2168}\,\sigma^* + \underset{[73.8]}{318{,}901}\,\frac{1}{RT}\right]$$

$$R^2 = 99.98\% \qquad [15]$$

with

$$w_1 = \frac{1}{1+\exp[5.2120(\sigma^* + 0.3355)]}$$

These estimates suggest that when $\sigma^*_{(kink)} = -0.3355$ (i.e. when $\sigma/\sigma_{TS} = 0.49$), two different creep deformation mechanisms (or two different groups of mechanisms) contribute equally towards the overall creep strain. Notice this break point is estimated slightly differently

to that in the general model above. This is shown by $w_1 = 0.5$ at this stress boundary in Figure 5. Given the above interpretation that can be given to the weight w_1, it can also be seen from this figure that when $\sigma^* = 0.1$, about 90% of the observed creep strain is attributable to one of these mechanisms or group of mechanisms, whilst the other group of mechanisms dominates (90% domination) when $\sigma^* = -0.75$. So if the explanation given by Wilshire and Scharning [4] is correct, these estimates suggest that once σ^* has reached 0.1, 90% of the observed creep strain is attributable to dislocation movements within grain boundaries, whilst once σ^* has reached -0.75, 90% of the observed creep strain is attributable to dislocation movements within the crystal structure itself. When $\sigma^* = -0.3355$, these regions contribute equally to creep deformation.

Fig. 5 - The dominance of different deformation mechanisms at different stresses for 1Cr-1Mo-0.25V steel at 723K (450°C) to 948K (675°C). (Stress σ is in MPa).

Again student t values are shown in parenthesis and this model is capable of explaining over 99.9% of the variation in the log times to failure. The t values reveal that all the parameters are significantly different from zero at the 5% significance level. More than that, these t values imply that the 95% confidence intervals for each of the parameter estimates are:

$$a_1 \in (-16.65 \text{ to } -12.28) \quad ; \quad a_2 \in (-29.42 \text{ to } -27.01)$$

$$b_1 \in (4.82 \text{ to } 6.21) \quad ; \quad b_2 \in (3.97 \text{ to } 4.46)$$

$$d_1 \in (196{,}472 \text{ to } 227{,}197) \quad ; \quad d_2 \in (310{,}385 \text{ to } 327417)$$

so that in the two identified regimes, the activation energies are significantly different from each other, as are the values for u and k_1 implied by the above intervals for b_i and a_i. So again, based on the Wilshire and Scharning explanation, the activation energy associated with grain boundaries is between 196 and 227 kJmol^{-1} with 95% certainty, whilst the activation energy associated with the crystal structure is between 310 and 327 kJmol^{-1} with 95% certainty – which is statistically significantly higher.

Figure 6 shows the life time predictions given by Eq. [15] at 823K (550°C) and 873K (600°C), and for comparison purposes these are shown alongside those given by the original Wilshire predictions Eq. [9a]. All the unwanted discontinuities in these iso-thermal predictions are now removed by this approach. More importantly, the predictions at 823K (550°C) are much better – running now through the mid points of the observed failure times at the lowest stresses. At 873K (6000°C) the two predictions are very similar.

Fig. 6 - Predicted times to failure obtained using Eq. 9a and Eq. 15 for specimens tested at 823K (550°C) and 873K (600°C).

VIII. CONCLUSIONS

The proposed new estimation framework provided confirmation that the original identification by Wilshire and Scharning of a break point with respect to stress, rather than

temperature, for 1Cr-1Mo-0.25V steel was indeed correct (as shown by $(1/RT)_{kink}$ = min(1/RT)). However, this modified model revealed some difference between that original study and this illustration. First, the break point in this study was estimated to occur at a normalised stress of 0.49 rather than 0.44. Secondly, the predictions made at 823K (550^{o}C) were much more in agreement with the experimental data – especially at the all-important lower stresses that correspond more closely to the in service stresses experienced by these materials in power plants. Third, the model identifies a big difference in the activation energies associated with dislocation movements along grain boundaries and within the main crystal structure – a difference not revealed by the original Wilshire study. Finally, the modified model provides additional information on the relative contribution of deformation within these two regions to total creep strain as stress varies.

REFERENCES

1. ASME Boiler & Pressure Vessel Code, Sec. II, Part D, Appendix I, ASME (2004).
2. J. Hald: Creep strength and ductility of 9 to 12% chromium steels, *Materials at High Temperatures*, 21, 2004, 41–46.
3. B. Wilshire, A.J. Battenbough: Creep and creep fracture of polycrystalline copper, *Materials Science and Engineering A,* 443, 2007, 156-166.
4. B. Wilshire, P.J. Scharning: Prediction of long term creep data for forged 1Cr-1Mo-0.25V steel, *Materials Science and Technology*, 24(1), 2008, 1-9.
5. B. Wilshire, M. Whittaker: Long term creep life prediction for grade 22 (2.25Cr-1Mo) steels, *Materials Science and Technology*, 27(3), 2011, 642-647.
6. B. Wilshire, P.J. Scharning: A new methodology for analysis of creep and creep fracture data for 9-12% chromium steels, *International Materials Reviews*, 53(2), 2008, 91-104.
7. A. Abdallah, K. Perkins, S. Williams: Advances in the Wilshire extrapolation technique - Full creep curve representation for the aerospace alloy Titanium 834, *Materials Science and Engineering A*, 550, 2012, 176-182.
8. M.T. Whittaker, M. Evans, B. Wilshire: Long-term creep data prediction for type 316H stainless steel, *Materials Science and Engineering A*, 552, 2012, 145-150.
9. D. Allen, S. Garwood: Energy Materials-Strategic Research Agenda. Q2, *Materials Energy Review*, IoMMH London 2007.
10. F.C. Monkman, N.J. Grant: An empirical relationship between rupture life and minimum creep rate: Deformation and Fracture at Elevated Temperature, eds. N. J. Grant and A. W. Mullendore, MIT Press Boston 1963.
11. National Institute for Materials Science, Creep Data Sheet No. 9b, 1990.
12. M. Evans: Formalisation of the Wilshire - Scharning methodology to creep life prediction with application to 1Cr-1Mo-0.25V rotor steel, *Materials Science and Technology,* 26(3), 2010, 309-317.
13. M. F. Ashby, D.R.H. Jones: Engineering Materials 1: An introduction to their properties & applications, Butterworth-Heinemann, Oxford 1996.

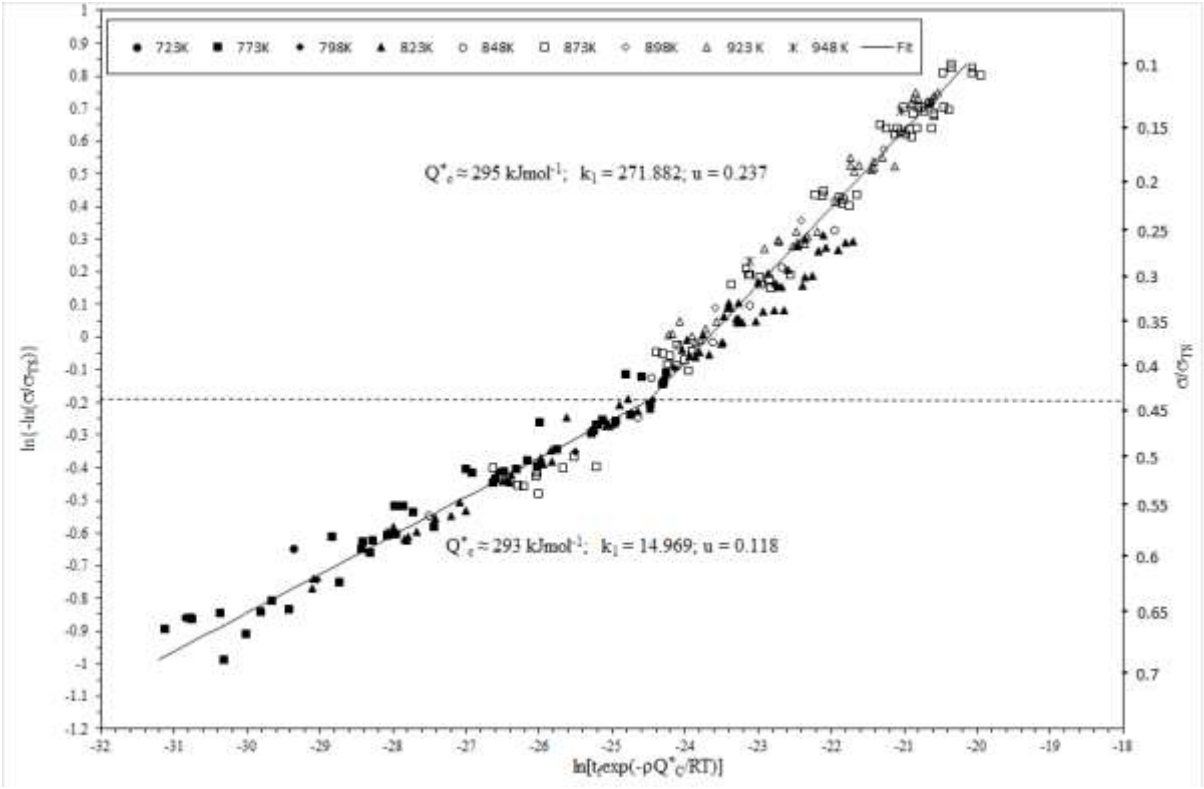

Fig. 1 - Dependence of $\ln[t_f \exp(-\rho Q_c^*/RT)]$ on $\ln[-\ln(\sigma/\sigma_{TS})]$ for 1Cr-1Mo-0.25V steel at 723K (450°C) to 948K (675°C). (Failure time t_f is in seconds, stress σ is in MPa, and Temperature T is the absolute temperature).

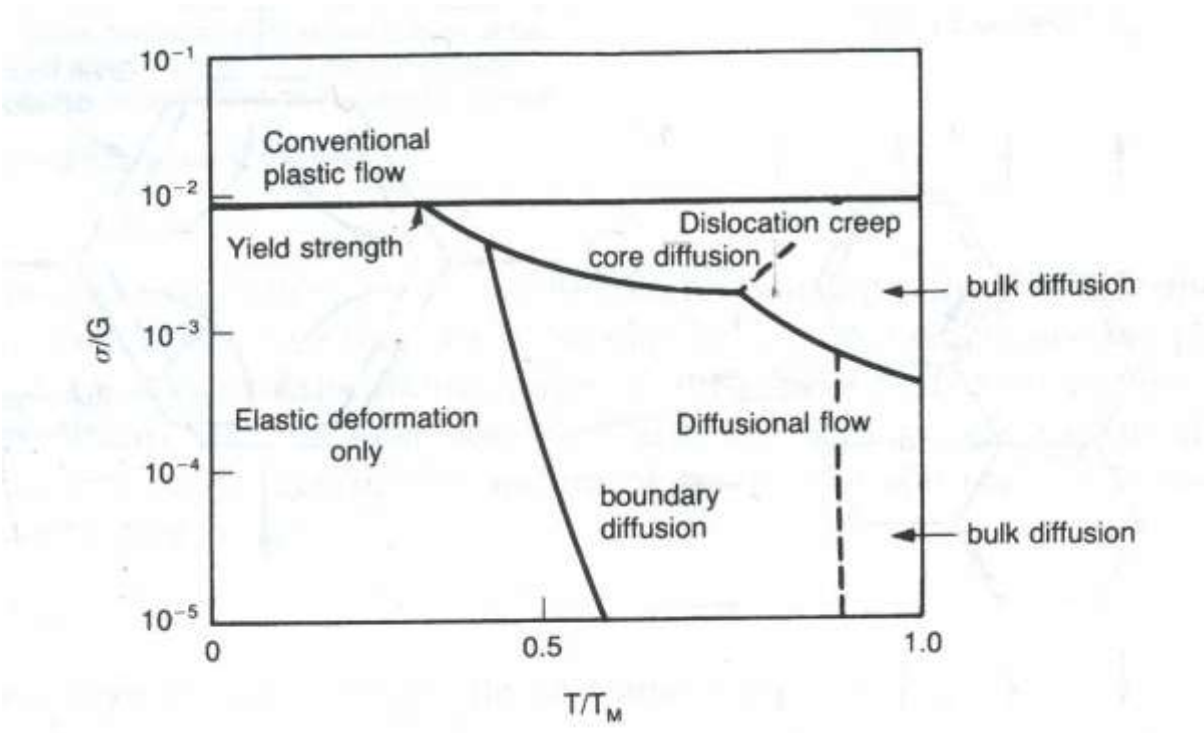

Fig. 2 - Deformation mechanisms at different stresses and temperatures. Ashby and Jones [13].

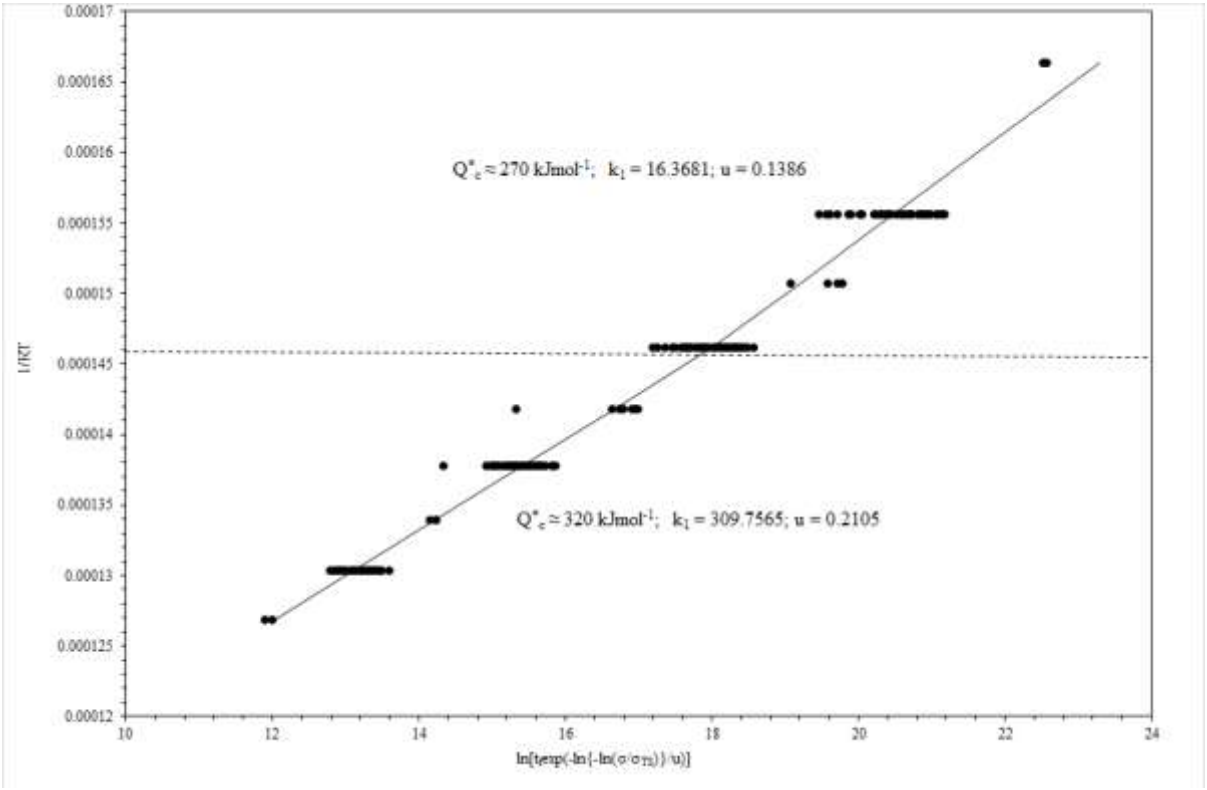

Fig. 3 - Dependence of $\ln[t_f.\exp(-\sigma^*/u)]$ on $1/RT$ for 1Cr-1Mo-0.25V steel at 723K (450ºC) to 948K (675ºC). (Failure time t_f is in seconds, stress σ is in MPa, and Temperature T is the absolute temperature).

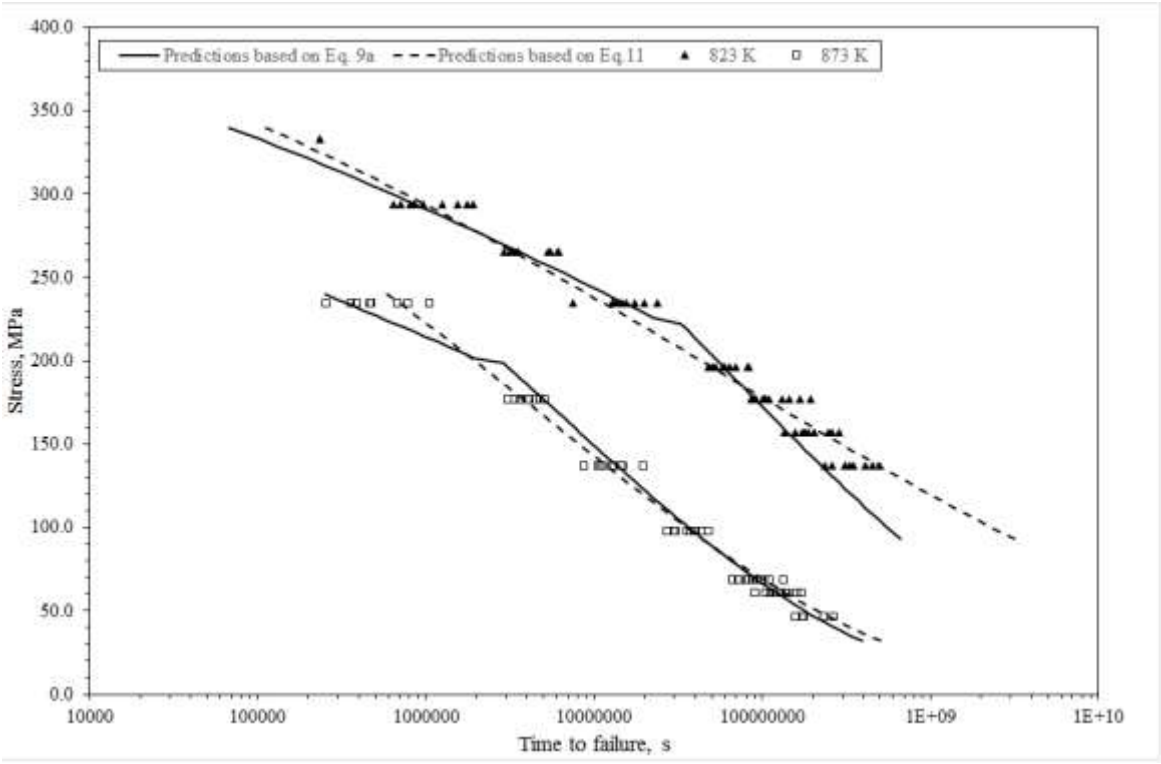

Fig. 4 - Predicted times to failure obtained using Eq. 9a and Eq. 11 for specimens tested at 823K (550ºC) and 873K (600ºC).

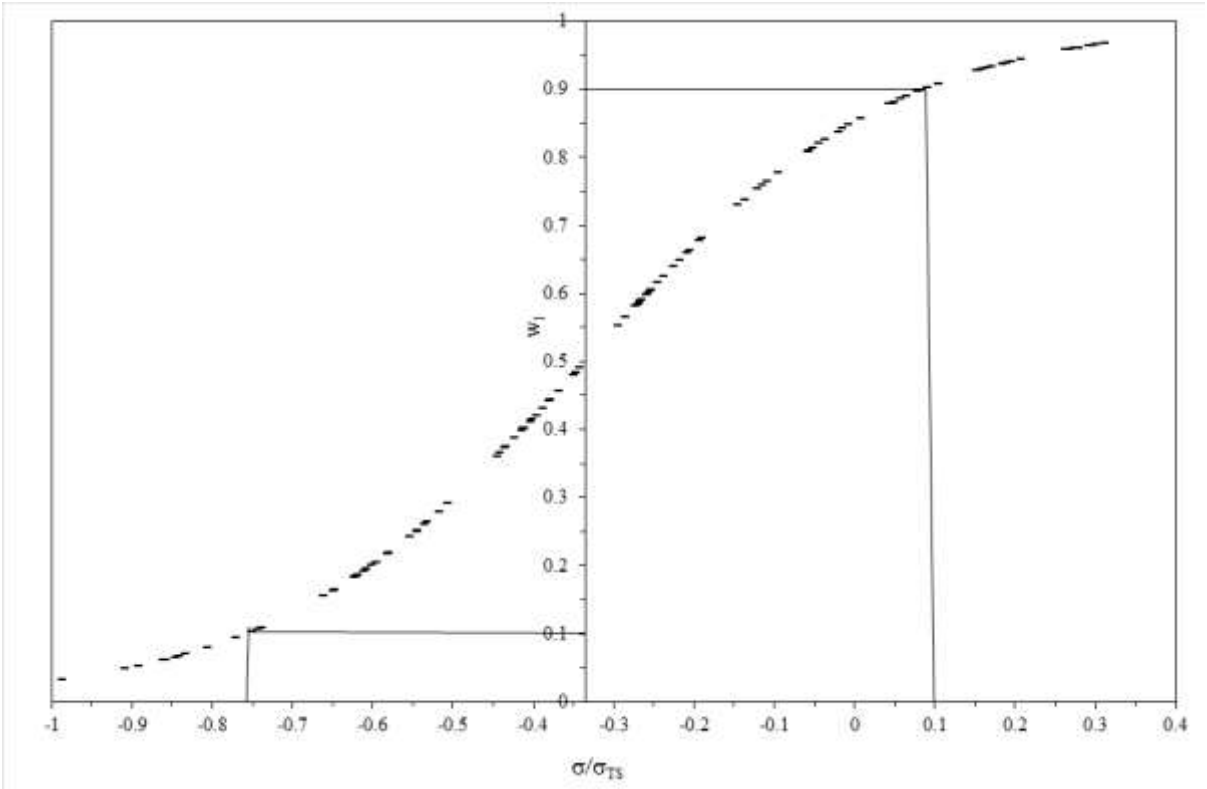

Fig. 5 - The dominance of different deformation mechanisms at different stresses for 1Cr-1Mo-0.25V steel at 723K (450ºC) to 948K (675ºC).

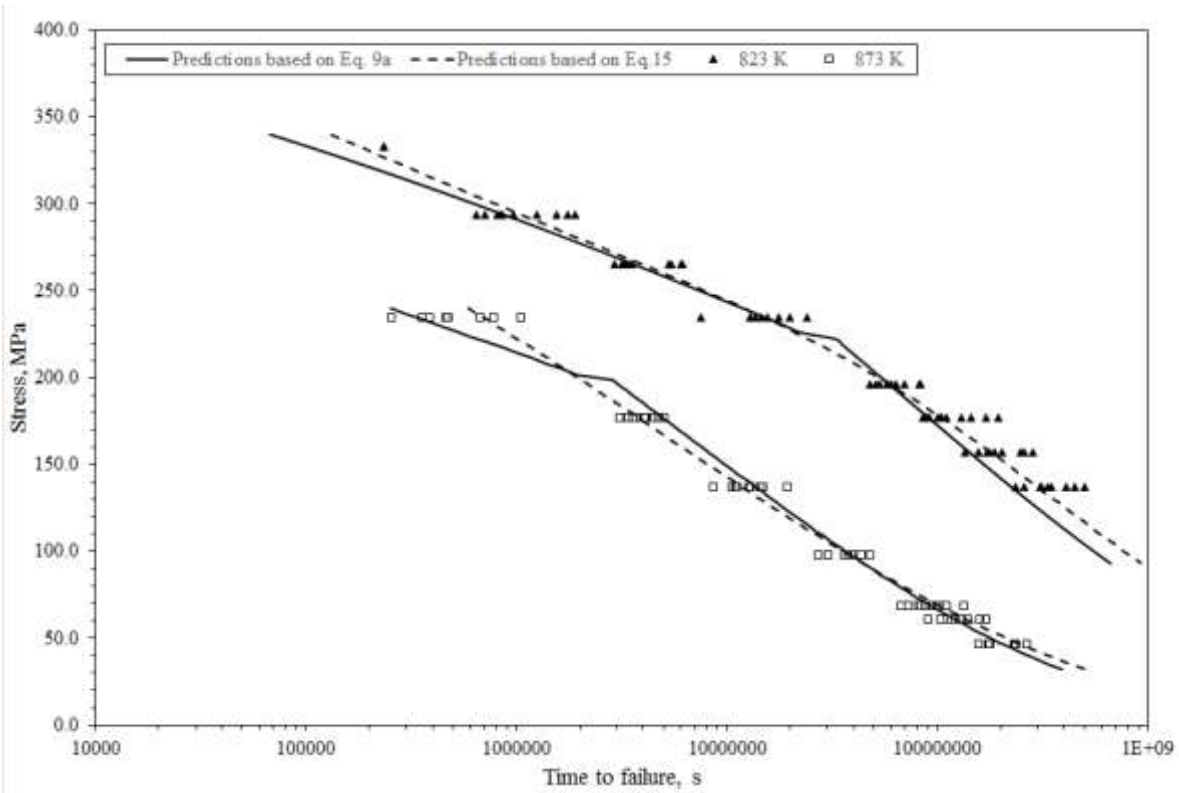

Fig. 6 - Predicted times to failure obtained using Eq. 9a and Eq. 15 for specimens tested at 823K (550ºC) and 873K (6000ºC).

Table I. Composition and Heat Treatment of 1Cr-1Mo -0.25V Steel

Batch code	Chemical composition (mass percent)											
	C	Si	Mn	P	S	Ni	Cr	Mo	Cu	V	Al	N
Requirements	0.25 - 0.35	0.15 - 0.35	≤ 1.0	≤ 0.015	≤ 0.018	≤ 0.75	0.9-1.5	1.0-1.05	-	0.2-0.3	-	-
VaA	0.28	0.20	0.72	0.015	0.012	0.32	1.02	1.12	0.20	0.27	0.002	0.0075
VaB	0.28	0.18	0.75	0.012	0.009	0.32	1.00	1.25	0.14	0.26	0.002	0.009
VaC	0.29	0.20	0.75	0.010	0.009	0.34	1.00	1.25	0.14	0.26	<0.002	0.0075
VaD	0.3	0.28	0.72	0.014	0.006	0.35	0.93	1.22	0.16	0.21	0.002	0.0093
VaE	0.3	0.26	0.79	0.016	0.015	0.32	1.03	1.13	0.19	0.23	<0.002	0.0085
VaG	0.29	0.26	0.76	0.009	0.007	0.45	1.12	1.18	0.07	0.23	0.002	0.0103
VaH	0.29	0.26	0.77	0.009	0.007	0.46	1.12	1.20	0.08	0.23	<0.002	0.0095
VaJ	0.29	0.21	0.66	0.010	0.008	0.51	1.07	1.29	0.06	0.23	0.002	0.0097
VaR	0.3	0.27	0.70	0.012	0.012	0.44	1.10	1.35	0.11	0.27	0.002	0.0082